Laser-Electron Photon Beamline for Quark Nuclear Physics (BL33LEP)

1. Introduction

BL33LEP is a contract beamline of the Research Center for Nuclear Physics (Osaka University) for investigating quark nuclear physics. SPring-8 is the only facility where a high intensity LEP beam above 2 GeV can be obtained. We mainly describe the physics and the detector system with the GeV photons in this report. Other information may be found elsewhere [1,2].

2. LEPS Facility

The beamline has a 7.8 m long straight section between two bending magnets (Fig.1). Polarized laser photons are injected from a laser hutch toward the straight section, where Backward-Compton scattering (BCS) [3] of the laser photons by the 8 GeV electron beam takes place:

$$e_0 + \omega_0 \rightarrow e' + \omega',$$

where e_0, ω_0, e', ω' are stored electron, laser photon, scattered electron, and LEP, respectively. The LEP beam is transferred to the experimental hutch, 60 m downstream of the straight section. The LEP beam size is ~ 1 cm on the target. The intensity, position, and polarization of the laser lights which do not interact with the electron beam are monitored at the upstream end of the beamline. Figures 2-(a) ~ (c) show the LEP beam characteristics.

The beam energy is determined by measuring the energy of a recoil electron with a tagging counter. The tagging counter is located at the exit of the bending magnet after the straight section. It consists of multiple layers of a 0.1 mm pitch silicon strip detector (SSD) and plastic scintillator hodoscopes. Electrons in the energy region

Fig. 1. Plan view of the Laser-electron photon facility at SPring-8 (LEPS).

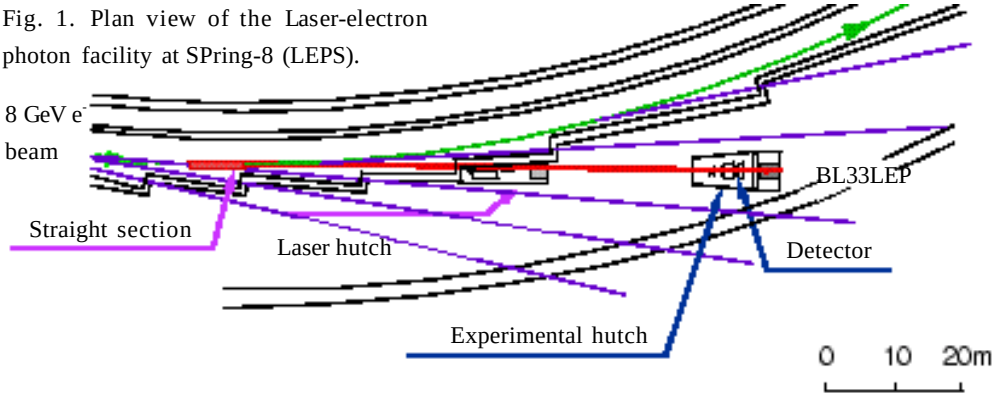

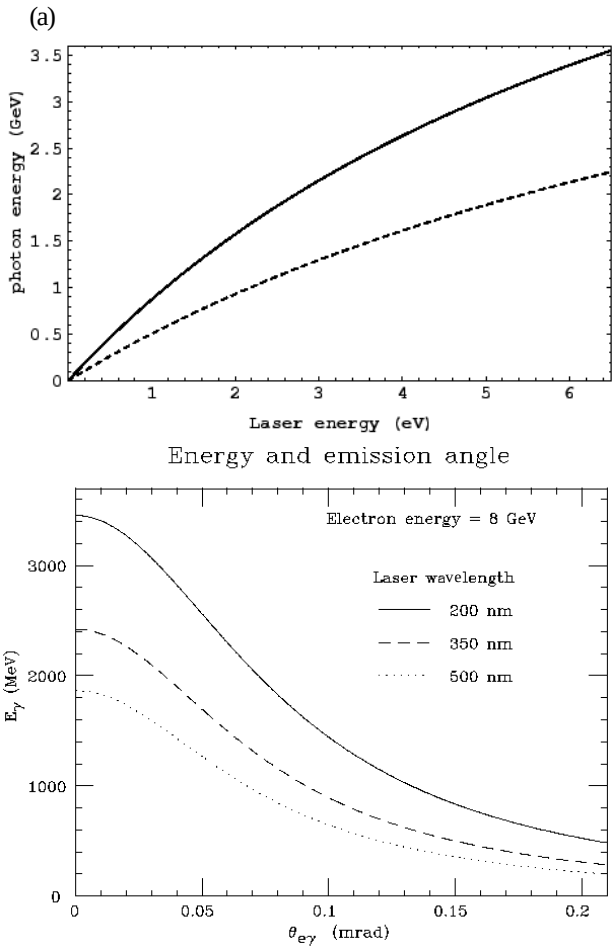

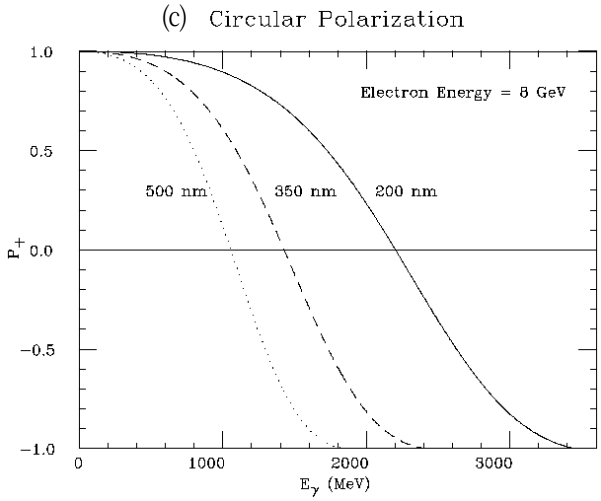

Fig. 2. (a) Laser photon energy versus maximum LEP energy with an 8 GeV (solid line) and 6 GeV (dashed line) electron beam. (b) Scattered angle versus LEP energy. (c) Relation between polarization and photon energy. Laser photons at various wavelengths are assumed to have 100 % circularpolarization.

of 4.5 - 6.5 GeV are detected by the counter. The corresponding photon energy is 1.5 - 3.5 GeV. The position resolution of the system is much better than the required resolution. The resolution (RMS) of 15 MeV in the photon beam energy determination comes from the energy spread of the electron beam and uncertainty of a photon-electron interaction point.

In the first stage, we use a conventional Ar laser. The 25 W Ar CW-laser has a 2 W output at 351 nm (3.5 eV). The maximum energy of the BCS photon with this laser light is 2.4 GeV. If we use a multi-line mode around 351 nm, the laser output power is about 5 W. The corresponding intensity of the BCS photon beam amounts to 10^7 photons/sec, which is the maximum intensity approved for the project.

3. Physics Programs

In this section, we describe a few physics programs which can be studied with a charged particle spectrometer.

It is well known that all the hadron-hadron total cross sections (including a γp total cross section) in a wide energy range are reproduced very well in terms of two s-dependent terms with $s^{-0.5}$ and $s^{0.08}$ dependences, where s is the Mandelstam s variable [4]. The Reggeon exchange model clearly suggests that the $s^{-0.5}$ term originates from the ρ meson ($T=1, J^{\pi} = 1^-$.) trajectory. On the other hand, the $s^{0.08}$ term requires the introduction of a Pomeron trajectory [5] whose $\alpha(t=0)$ must be 1.08. One can identify the Pomeron trajectory with a multi-gluon exchange since the first particle state on the trajectory appears at $m^2 \sim 4$ GeV^2 with $J = 2$ (2^{++} glueball).

At high energies, the diffractive photoproduction of a vector meson from a proton target is well described as a Pomeron-exchange process in the framework of the Regge theory and of the Vector Dominance Model (VDM) [6]; a high energy photon converts into a vector meson and then it is scattered from a proton by an exchange of the Pomeron [7]. Within QCD, interactions between hadrons can be due to quark- and gluon- exchanges. Phenomenologically, we know that the quark-exchange processes can be simulated by meson-exchange, which can be calculated from effective Lagrangians based on QCD. This has been a very successful way of understanding various photoproduction data at low energies. On the other hand, the gluon-exchange mechanism is poorly understood.

For the ϕ production, the meson-exchange contribution is small because the couplings of the ϕ meson to other non-strange mesons are weak due to OZI suppression. Precise measurements of $d\sigma/dt$ and spin observables at low energies will provide important information on the Pomeron exchange dynamics through interferences with the meson exchange amplitudes [8]. Moreover, the ϕ production measurements near the threshold may reveal the existence of another gluon-exchange trajectory (a 0^{++} glueball trajectory) whose contribution falls off rapidly at high energies. In the measurement of ϕ production, one can also address the question of the s·s-bar components in a nucleon. Again, polarization data obtained by using polarized photons are crucial. Spin observables magnify small amplitudes hidden in a dominant amplitude by interference effects. The interference between a Pomeron-exchange amplitude and a small amplitude due to a direct knockout of s·s-bar in the nucleon may cause a large asymmetry of the production cross sections between the spin parallel and anti-parallel configurations of the polarized photon and polarized nucleon [9].

A photoproduction of $\Lambda(1405)$ from a proton is also of great interest. A recent theoretical work within the framework of a chiral unitary model treats the $\Lambda(1405)$ as a dynamically generated KN resonance. The detection of K^+ from the $\gamma p \rightarrow K^+\Lambda(1405)$ is sufficient to determine the shape and strength of the $\Lambda(1405)$ theoretically [10].

The final topic is a search for a σ meson via a Primakov process [11]. In this study, we search for enhancement of two-pion production from a heavy target in a very forward angle, with a small invariant mass, and in a small momentum transfer region. The enhancement is expected if there is a state with positive charge parity and a wide width which couples both to two gammas and two pions.

4. Detector

The LEPS detector shown in Fig. 3 consists of charged particle tracking counters, a dipole magnet, and a time-of-flight wall. The design of the detector is optimized for a ϕ photoproduction in forward angles. It has a large forward acceptance and good coverage of momentum transfer t for the photoproduction, as shown in Fig. 4.

The opening of the dipole magnet is 135 cm wide and 55 cm high. The length of the pole is 60 cm, and the field strength at the center is 1 T. The vertex detector consists of two planes (x- and y-) of single-sided SSDs (SVTX) and five planes (x,x',y,y',u) of multi-wire drift chamber (DC1), which are located upstream of the magnet. The stereo ambiguity (pairing ambiguity) for two-track events are solved with DC1. The thickness of each SSD is 300 μm, which results in angle spread (σ) of ~ 1 mrad. The corresponding deterioration in 2-kaon invariant mass and momentum transfer t measurements are 300 keV and 2×10^{-3} GeV^2 respectively. Two sets of MWDCs (DC2 and DC3) are located downstream of

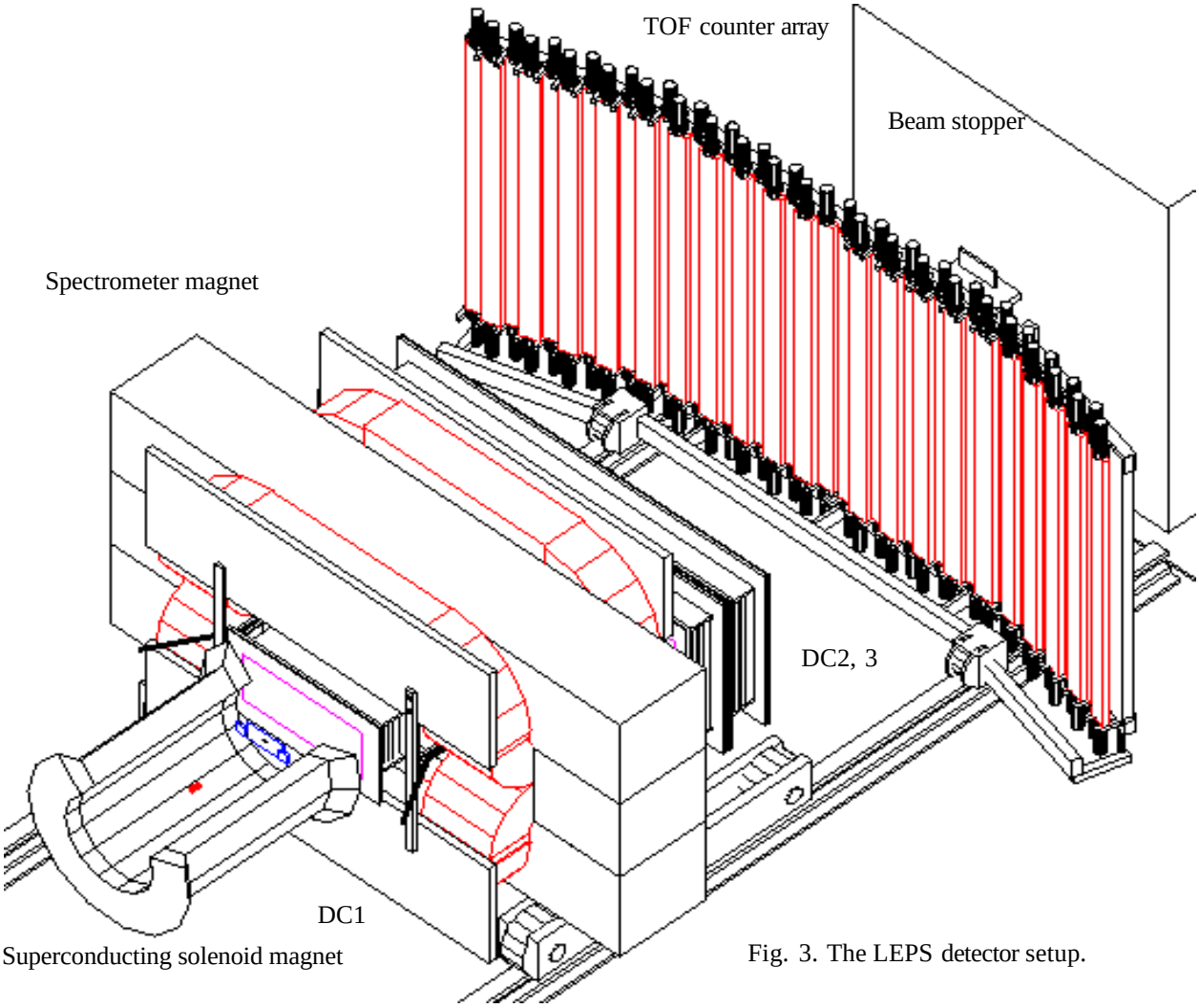

Fig. 3. The LEPS detector setup.

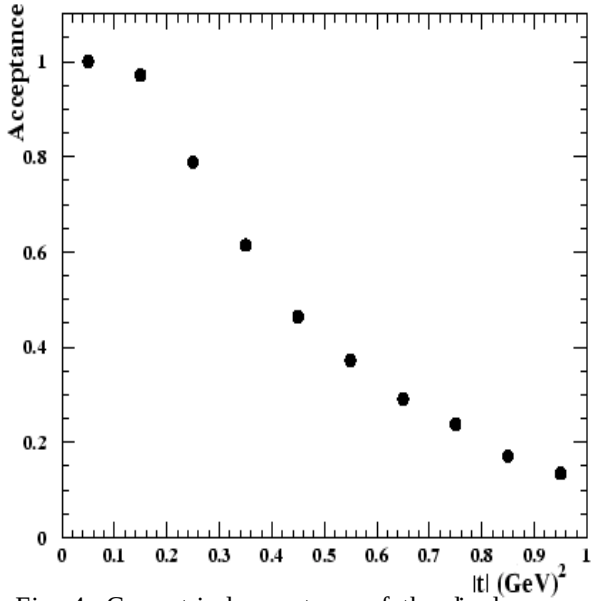

Fig. 4. Geometrical acceptance of the dipole magnet for the reaction $\gamma+p \rightarrow \phi+p$, $\phi \rightarrow K^+K^-$ at $E_\gamma = 2.4$ GeV as a function of a momentum transfer |t|. Both Kaons are required to go through the magnet. The distance between a target and the magnet center is 90 cm.

the magnet. The active area size of DC2 and DC3 is 200 cm(W) × 80 cm(H). Each set has 5 planes: x,x',y,y', and u(v) in order to solve both left-right ambiguity and stereo ambiguity locally. Figure 5 shows the momentum resolution as a function of a momentum.

The identification of momentum analyzed particles is performed by measuring a time of flight from a target to the TOF wall. The start signal for the TOF measurement is provided by an RF signal from the 8-GeV ring, where electrons are bunched every 2 nsec (508MHz) at a width (σ) of 17 psec. Since the speeds of both the electron beam and a laser-electron photon are the same, the arrival time of the laser-electron photon at the target is synchronized with the RF signal. A stop signal is provided by the TOF wall consisting of 40 plastic scintillator bars with a dimension of 4 cm (T) ×12 cm (W) × 200 cm (L). The resolution of the TOF counter is less than 100 psec. When the TOF wall is located at 3 m from the magnet, a flight-length of a charged particle is about 4 m. In this case, the detector has the capability of 4-σ K/π separation up to 2 GeV/c.

A φ meson is identified through the reconstruction of

the KK invariant mass. The typical mass resolution is 600 keV, which is much smaller than the ϕ width. The measurement error of a momentum transfer is about 0.01 GeV^2, and it mainly comes from the measurement error of the incident photon energy. The elastic ϕ photoproduction from a proton and a quasi-free ϕ photoproduction from a nucleus are separated by reconstructing a recoiled target mass from the incident photon energy and the energy momentum of a ϕ. Figure 6 shows the reconstructed mass distribution by simulation. The narrow peak at the proton mass corresponds to the elastic production, and the broad tail corresponds to the quasi-free production. The broadening is due to a Fermi momentum of a nucleon in a nucleus.

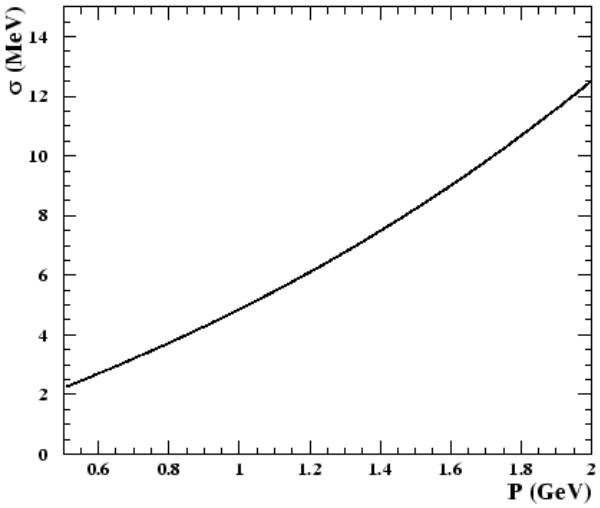

Fig. 5. The overall momentum resolution (σ MeV) as a function of a momentum in GeV.

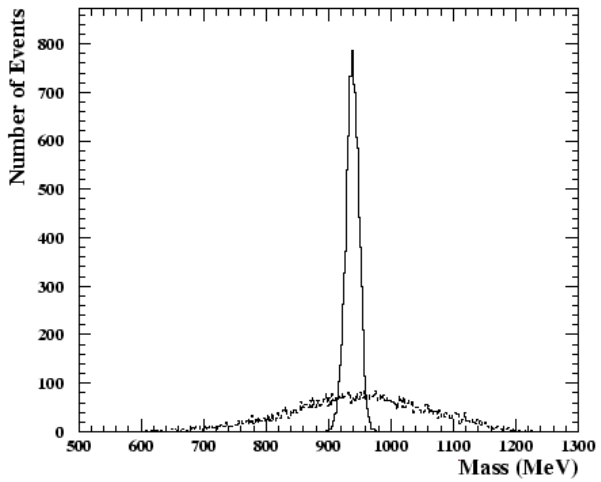

Fig. 6. The target mass distribution reconstructed from the incident γ energy and the ϕ momentum for ϕ photoproduction from a proton (solid) and a nucleus (dashed).

The beam intensity and profile during experiments are monitored by a beam monitor consisting of a pre-radiator to convert a photon into an e^+e^- pair, a thin plastic scintillation counter, and SSD counters.

For future upgrade, developments of an aerogel cherenkov counter, a γ counter, and a polarized target are in progress.

5. Status and Schedule

Replacement of the vacuum chambers in the storage ring and the construction of the beamline and the laser hutch were completed in September 1998. The laser system was installed during the winter shutdown of 1998. The construction of the experimental hutch and the detector system will be completed by the end of March 1999. The commissioning of the Laser-electron-photon beam will be carried out from May to July 1999. Then, the first test experiment will begin in September 1999.

Takashi Nakano
(Osaka University)

References

[1] S. Daté *et al.*, SPring-8 Annual Report 1995,172.(1997)., Y. Ohashi *et al.*, SPring-8 Annual Report 1997,172 (1997).
[2] T. Nakano, in Proceedings of Nuclear Physics Frontiers with Electro-Weak Probes, Osaka, Japan, 1996, edited by H. Toki *et al.* M. Fujiwara, T. Kinashi, and T. Hotta, J. Jpn. Soc. for Synchrotron Rad. Res. **10(**1), (1997) 23.
[3] R. H. Milburn, Phys. Rev. Lett., **10** (1963) 75.
[4] A. Donnachie and P. V. Landshoff, Phys. Lett., **B 296** (1992) 227.
[5] I. Y. Pomeranchuk, Sov. Phys., **7**, (1958) 499.
[6] J. J. Sakurai, Ann. Phys. **11** (1960) 1; J.J. Sakurai, Phys. Rev. Lett., **22** (1969) 981.
[7] T. H. Bauer *et al.*, Rev. Mod. Phys., **50** (1978) 261.
[8] A. I. Titov *et al.*, nucl-th/9812074.
[9] A. I. Titov *et al.*, Phys. Rev. Lett., **79** (1997) 1634; A. I. Titov *et al.*, Phys. Rev. **C58** (1998) 2429.
[10] E. Oset, in this proceedings.
[11] H. Shimizu, private communications.